

Multiply Confined Nickel Nanocatalysts Produced by Atomic Layer Deposition for Hydrogenation Reactions**

Zhe Gao, Mei Dong, Guizhen Wang, Pei Sheng, Zhiwei Wu, Huimin Yang, Bin Zhang, Guofu Wang, Jianguo Wang, and Yong Qin*

Abstract: To design highly efficient catalysts, new concepts for optimizing the metal–support interactions are desirable. Here we introduce a facile and general template approach assisted by atomic layer deposition (ALD), to fabricate a multiply confined Ni-based nanocatalyst. The Ni nanoparticles are not only confined in Al₂O₃ nanotubes, but also embedded in the cavities of Al₂O₃ interior wall. The cavities create more Ni–Al₂O₃ interfacial sites, which facilitate hydrogenation reactions. The nanotubes inhibit the leaching and detachment of Ni nanoparticles. Compared with the Ni-based catalyst supported on the outer surface of Al₂O₃ nanotubes, the multiply confined catalyst shows a striking improvement of catalytic activity and stability in hydrogenation reactions. Our ALD-assisted template method is general and can be extended for other multiply confined nanoreactors, which may have potential applications in many heterogeneous reactions.

Traditional heterogeneous catalysts, often consisting of metal nanoparticles supported on oxide solids, are used in a wide variety of industrial and environmental applications. To improve our capability of designing highly efficient catalytic systems, new concepts for optimizing the metal–support interactions are desirable.^[1] Confining metal nanoparticles in porous materials or carbon nanotubes has proven to be an alternative approach for the design of a novel class of heterogeneous catalysts with enhanced activity and stability.^[2] Confined catalysts utilizing metal oxide nanotubes have also been explored.^[3] In terms of maximizing the metal–oxide interaction, the oxide nanotube-confined structure is not the most ideal structure if the enhanced performance is caused only by the incorporation of metal nanoparticles inside these oxide nanotubes, namely spatial confinement effect. Rational

design and engineering of metal–oxide interfaces are critical in developing highly efficient catalytic systems.^[4]

Herein, we employed a facile template-assisted method based on atomic layer deposition (ALD) to synthesize Ni nanoparticles not only confined in Al₂O₃ nanotubes, but also confined in the cavities of Al₂O₃ interior wall, to maximize the metal–support interfaces. The increased interfacial sites and protecting nanotubes greatly improve the activity and stability of confined catalysts for hydrogenation reactions of cinnamaldehyde and nitrobenzene.

ALD is a powerful technique for depositing nanoparticles or thin films with outstanding advantages including precise control of size and thickness and excellent uniformity.^[5] It has emerged as a powerful tool for the atomically precise design and synthesis of catalytic materials.^[6] Ni nanoparticles confined in Al₂O₃ nanotubes (Ni-in-ANTs) and Ni nanoparticles on Al₂O₃ nanotubes (Ni-out-ANTs) were obtained by ALD using carbon nanocoils (CNCs) as sacrificial templates (Figure 1). Compared with carbon nanotubes (CNTs), the

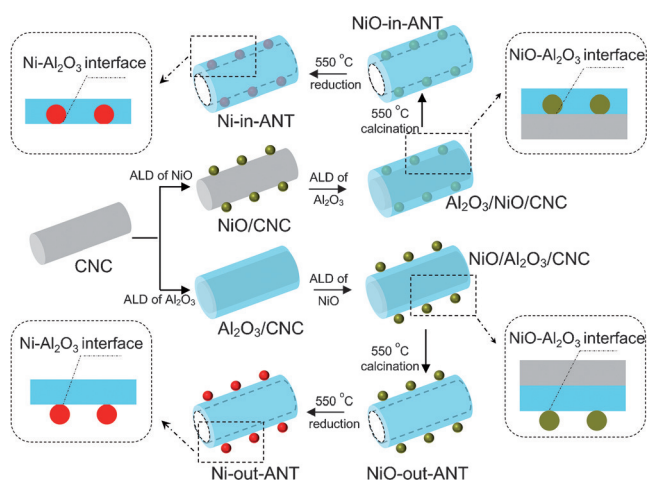


Figure 1. Preparation process of catalysts.

CNCs have lower annealing temperature for convenient removal and are more suitable for uniform ALD coating, because of their low thermal stability and abundant active groups on their surface.^[7] The ALD process was carried out in a hot-wall closed chamber-type ALD reactor. Al₂O₃ was deposited at 150 °C with trimethylaluminum and deionized H₂O as precursors. NiO was deposited with nickelocene and O₃ as precursors at 200 °C. Nickelocene were kept at 75 °C. For Ni-in-ANTs, NiO nanoparticles were first deposited onto CNCs with 150 ALD cycles. Here we used large cycle

[*] Dr. Z. Gao, Prof. M. Dong, Dr. G. Z. Wang, P. Sheng, Dr. Z. W. Wu, H. M. Yang, Dr. B. Zhang, G. F. Wang, Prof. J. G. Wang, Prof. Y. Qin State Key Laboratory of Coal Conversion Institute of Coal Chemistry, Chinese Academy of Sciences Taiyuan 030001 (China) E-mail: qinyong@sxicc.ac.cn

[**] We appreciate financial support from the National Natural Science Foundation of China (21173248, 21403272, 21227002, 21376256, and 51362010), the Hundred Talents Program of the Chinese Academy of Sciences, the Hundred Talents Program of Shanxi Province, and in-house projects of the State Key Laboratory of Coal Conversion of China (2013BWZ005). XAFS studies were carried out at BL14W1 beamline at the Shanghai Synchrotron Radiation Facility, Shanghai Institute of Applied Physics, China.

Supporting information for this article is available on the WWW under <http://dx.doi.org/10.1002/anie.201503749>.

numbers for NiO ALD to get larger Ni nanoparticles for convenient observation by transmission electron microscopy (TEM). Then the as-prepared NiO/CNCs were further coated by an amorphous Al₂O₃ film with a thickness of about 20 nm also by ALD, labeled as Al₂O₃/NiO/CNCs. In this case, NiO nanoparticles are confined in the cavities of Al₂O₃ shell. The CNCs templates were removed by subsequent calcination in air (Figure S1 in the Supporting Information). Finally, a reduction treatment produced Ni-in-ANTs. Here Ni nanoparticles are not only confined in Al₂O₃ nanotubes, but also confined in the cavities of Al₂O₃ interior wall. For Ni-out-ANTs, we just need exchange the deposition sequence of NiO nanoparticles and Al₂O₃ films. The subsequent calcination and reduction treatments are the same as described above. In this case, NiO or Ni nanoparticles are supported on the outer surfaces of Al₂O₃ wall.

TEM images of Ni-in-ANTs (Figure 2 A,B) and Ni-out-ANTs (Figure 2 D,E) clearly show their hollow structures. The average diameters of Ni nanoparticles are 6.1 and 6.2 nm for Ni-in-ANTs and Ni-out-ANTs, respectively. None of Ni nanoparticles are located on the outer surfaces of Al₂O₃ nanotubes for Ni-in-ANTs. This perfect encapsulation can hardly be obtained by traditional preparation methods. In contrast, all of Ni nanoparticles are loaded on the Al₂O₃ outer surfaces for Ni-out-ANTs. In principle, the Ni nanoparticles of Ni-in-ANTs are confined in the cavities of Al₂O₃ interior wall (Figure 1). However, this is visible only at the borderline of the perspective projection of the inner surface of the Al₂O₃ shell, because TEM is a 2D imaging technology (Figure 2 C). The Ni contents in the catalysts, measured by inductively coupled plasma-atomic emission spectrometry (ICP-AES), are 11.91% and 10.80% for Ni-in-ANTs and Ni-out-ANTs, respectively.

Selective hydrogenation of cinnamaldehyde (CA) was chosen to evaluate the catalytic performance of Ni-based catalysts. Figure 3 A shows the evolution of CA conversion with the reaction time up to 7 h for the catalysts. The reaction was carried out at 80°C and 2.0 MPa H₂ with 10 mg of catalyst in 30 mL of isopropyl alcohol, and 100 μL of cinnamaldehyde. It can be observed that Ni-in-ANTs exhibits a much higher activity than Ni-out-ANTs. After reaction for 10 min, the conversion of CA on Ni-in-ANTs reaches 4.2%, while the reaction product can hardly be detected for Ni-out-ANTs. After reaction for 7 h, the conversion of CA on Ni-in-ANTs reaches nearly 100%; in comparison, only 17.8% conversion is obtained on Ni-out-ANTs. Turnover frequency (TOF) is calculated on the basis of surface Ni atoms, which is determined according to the CO chemisorption (Table S1). The TOF values at initial times of 60 min are 0.42 and 0.08 s⁻¹ for Ni-in-ANTs and Ni-out-ANTs, respectively. Hydrogenation of CA to hydrocinnamaldehyde (HCA) is the main reaction (Figure S2).

The catalysts were reused to test their stabilities (Figure 3 B). The reaction time is 5 h for each run. Ni-in-ANTs appears as relatively stable; a slight decrease in the conversion appears after the catalyst was reused four times. The conversion of Ni-out-ANTs decreases sharply, only remaining 1.2% after being reused four times. HCA is the

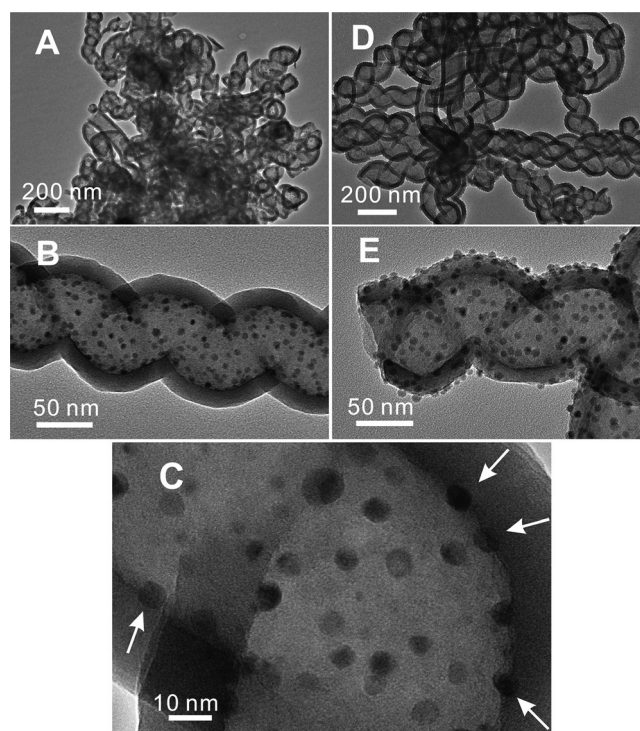


Figure 2. TEM images of A,B) Ni-in-ANTs and D,E) Ni-out-ANTs, and C) HRTEM image of Ni-in-ANTs.

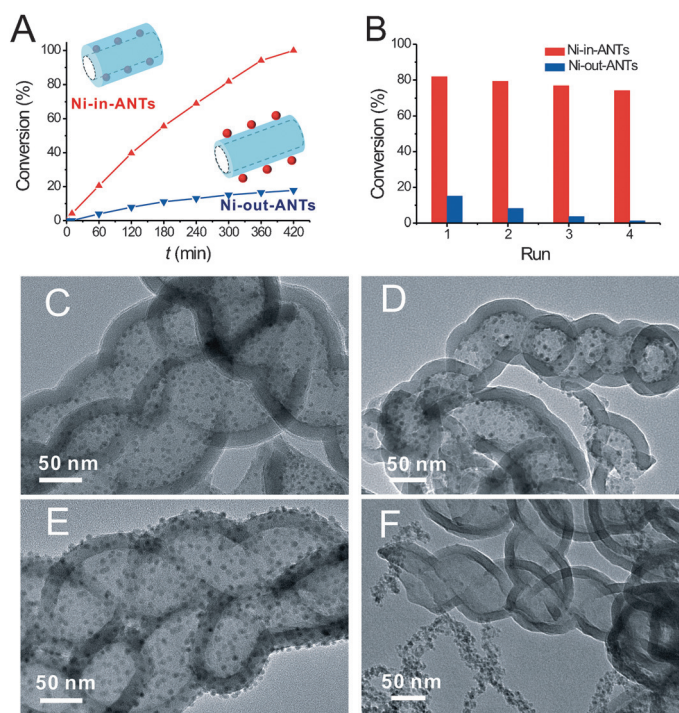


Figure 3. A) The evolution of CA conversion with reaction time and B) the recycling results for the catalysts in the hydrogenation of CA. TEM images of Ni-in-ANTs C) after reaction for 10 min and D) after the fourth run; and of Ni-out-ANTs E) after reaction for 10 min and F) after the fourth run.

main product during recycling test (Table S2). In general, the gradual detachment of nanoparticles from support is a main

reason responsible for the deactivation. After reaction for 10 min, Ni nanoparticles are still supported by Al_2O_3 nanotubes for both catalysts, indicating that no obvious detachment has happened in such a short time (Figure 3C,E). Note that this reveals that the difference of activity for the two catalysts is not essentially ascribed to detachment. Most of Ni nanoparticles are still confined in the Al_2O_3 nanotubes for Ni-in-ANTs after the fourth run (Figure 3D). However, after the fourth run, vast majority of Ni nanoparticles of Ni-out-ANTs are detached, forming large aggregates (Figure 3F). Leaching is another reason for deactivation of supported catalysts. The Ni contents in the reactant solvent (isopropyl alcohol) after the reaction, measured by ICP-AES, are 0.39 and 1.35 ppm for Ni-in-ANTs and Ni-out-ANTs, respectively. Based on the Ni contents in solution, the Ni content in the re-used catalysts (including the detached Ni particles) are 11.79% and 10.40% for Ni-in-ANTs and Ni-out-ANTs, respectively. These results suggest that Ni-out-ANTs underwent more leaching and much severer detachment than Ni-in-ANTs.

Ni-in/out-ANTs using 50 and 300 cycles of NiO ALD were also prepared (Figure S3). Similarly, Ni-in-ANTs shows higher activities than Ni-out-ANTs (Table S3). Ni-in-ANTs also presents much higher activities for the hydrogenation of nitrobenzene to aniline than Ni-out-ANTs (Table S4). Our ALD-assisted template method is general. It is also suitable for other templates such as CNTs (Figure S4).

The above results reveal that Ni-in-ANTs does possess greatly improved catalytic performance than Ni-out-ANTs. In order to elucidate the reasons, we performed further characterizations for these catalysts. The N_2 adsorption–desorption isotherms of NiO-in-ANTs and NiO-out-ANTs are almost overlapped (Figure S5), indicating that the two samples almost possess the same pore structure. Brunauer–Emmett–Teller (BET) surface areas of NiO-in-ANTs and NiO-out-ANTs samples are calculated to be 65.0 and 63.6 m^2g^{-1} , respectively. XRD patterns of the two reduced samples reveal the presence of metallic nickel after reduction (Figure S6). CO chemisorption experiments were used to measure the accessibility of Ni nanoparticles. The amount of CO adsorbed by Ni-in-ANTs (110.7 $\mu\text{molg}^{-1}\text{Ni}^{-1}$) is about 20% lower than on Ni-out-ANTs (135.0 $\mu\text{molg}^{-1}\text{Ni}^{-1}$) (Table S1, Figure S7). This reveals that Ni-out-ANTs has a higher Ni accessibility than Ni-in-ANTs.

The redox properties of NiO-in-ANTs and NiO-out-ANTs were compared through hydrogen temperature programmed reduction (H_2 -TPR) (Figure 4A). The profile of NiO-in-ANTs displays a small shoulder peak centered at 349 °C and a principal peak centered at 561 °C, corresponding to reduction of bulk NiO and the NiO interacting with Al_2O_3 , respectively. In contrast, for NiO-out-ANTs, the low-temperature peak at 394 °C becomes obvious, while the high-temperature peak at 546 °C shrinks. Quantification of the TPR curves shows that the total consumed hydrogen of NiO-in-ANTs (1.93 $\text{mmolH}_2\text{g}^{-1}$) exceeds that of NiO-out-ANTs (1.46 $\text{mmolH}_2\text{g}^{-1}$), which can be attributed to spillover

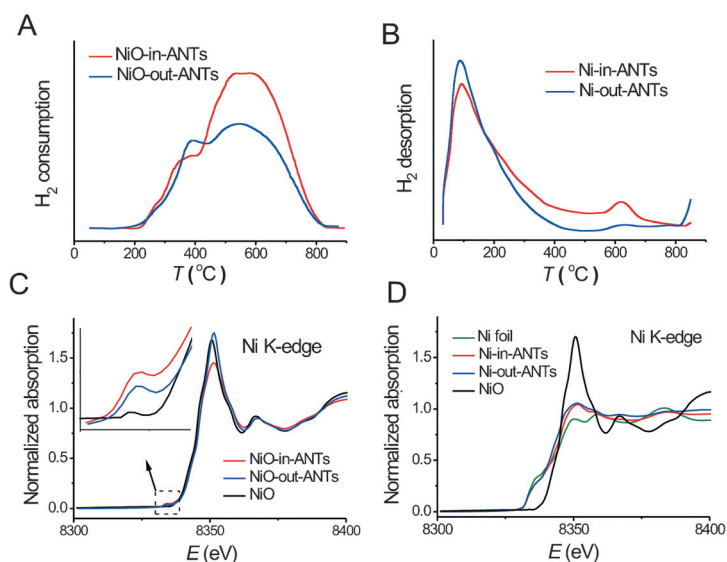


Figure 4. A) H_2 -TPR profiles of NiO-in/out-ANTs; B) H_2 -TPD profiles of Ni-in/out-ANTs; C) The normalized XANES of NiO-in/out-ANTs and reference sample; D) The normalized XANES of Ni-in/out-ANTs and reference samples. The inset in (C) is the amplified image of the pre-edge part of the XANES spectra.

hydrogen.^[8] At the high-temperature domain, the consumed hydrogen of NiO-in-ANTs is 1.7 times that of NiO-out-ANTs. These results suggest that, compared with NiO-out-ANTs, NiO-in-ANTs sample shows stronger NiO– Al_2O_3 interaction.

Hydrogen temperature programmed desorption (H_2 -TPD) tests of Ni-in-ANTs and Ni-out-ANTs were carried out (Figure 4B). Both the two TPD curves display two kinds of desorption peaks, indicative of the existence of different forms of surface hydrogen. The low-temperature desorption peaks (centered at 95 °C) are ascribed to the hydrogen adsorbed on the surface of metallic Ni, and the high-temperature desorption peaks above 500 °C (maxima at 620 °C) are assigned to spillover hydrogen.^[9] The intensity of low-temperature peak of Ni-in-ANTs is lower than that of Ni-out-ANTs, indicating Ni-in-ANTs shows a lower exposed fraction of Ni atom than that of Ni-out-ANTs, which is consistent with the CO chemisorption results. However, the intensity of high-temperature peak of Ni-in-ANTs is much higher than that of Ni-out-ANTs. This indicates that the hydrogen spillover effect for Ni-in-ANTs has been greatly enhanced, compared with Ni-out-ANTs.

X-ray absorption fine structure (XAFS) measurements were also employed to characterize the samples. From the X-ray absorption near-edge structure (XANES) spectra of NiO-in-ANTs and NiO-out-ANTs, it can be found that the intensity of the white line peak for NiO-in-ANTs is lower than that of NiO-out-ANTs (Figure 4C), and the intensity of the pre-edge absorption peak of NiO-in-ANTs is higher than that of NiO-out-ANTs (inset of Figure 4C). The k^2 -weighted Fourier transformed-extended X-ray absorption fine structure (FT-EXAFS) spectra of the two samples are presented in Figure S8A. The FT-EXAFS spectra on the first shell were fitted using NiO and NiAl_2O_4 as model compounds (Fig-

ure S8C,E). For NiO-in-ANTs, the ratio of the first peak intensity to the second peak intensity is larger than that of NiO-out-ANTs. This suggests that the interaction between NiO and Al₂O₃ of NiO-in-ANTs is stronger than that of NiO-out-ANTs, resulting in more surface NiAl₂O₄ species (Figure S6). For NiAl₂O₄, the first peak is stronger than the second one.^[10] The FT-EXAFS curve-fitting results (Table S5) further confirm this conclusion, which is also consistent with the H₂-TPR results.

From the XANES spectra of the reduced samples (Figure 4D), it can be seen that the Ni species were not fully reduced for the catalysts. The XANES spectra were simulated by a linear function of the references of the reduced (Ni foil) and oxidic (NiO) state to estimate the proportions of metallic Ni in the reduced samples (Figure S9). The XANES spectra can be reproduced by a simple sum of Ni foil and NiO references. The reduction degree of nickel for Ni-in-ANTs and Ni-out-ANTs are 80% and 77%, respectively, approximately equal (Table S6). Their *k*³-weighted FT-EXAFS spectra are presented in Figure S8B. The FT-EXAFS spectra on the first shell can be fitted well using NiO and Ni as model compounds (Figure S8D,F, and Table S7).

From all above characterizations, it can be concluded that Ni-in-ANTs and Ni-out-ANTs almost possess the same pore structure, thickness of Al₂O₃ shell and size of Ni nanoparticles, nickel content, and reduction degree of nickel. However, Ni-in-ANTs shows greatly enhanced catalytic performance compared with Ni-out-ANTs. This can be ascribed to the increased interfacial sites and protecting nanotubes.

First, from the H₂-TPR and XAFS results of NiO-in-ANTs and NiO-out-ANTs, it can be concluded that the interaction between NiO and Al₂O₃ of NiO-in-ANTs is stronger than that of NiO-out-ANTs. This is due to the larger interface of NiO-in-ANTs than that of NiO-out-ANTs. For the reduced samples, the CO chemisorption and H₂-TPD results suggest that Ni-out-ANTs show a higher Ni accessibility than Ni-in-ANTs, consistent with the fact that Ni nanoparticles are confined in the cavities of Al₂O₃ interior wall for Ni-in-ANTs (Figure 2C). The confinement of the cavities of Al₂O₃ interior wall creates more Ni–Al₂O₃ interfacial sites. The spillover of the dissociated hydrogen species is highly dependent on the metal–support interface.^[11] The hydrogen spillover effect for Ni-in-ANTs has been greatly enhanced, as is confirmed by H₂-TPD analysis. It is well known that hydrogen spillover can exert a great influence on the catalytic activity in hydrogenation reactions.^[12] In a word, the greatly improved catalytic activity of Ni-in-ANTs can be ascribed to its increased interfacial sites, which enhance the hydrogen spillover effect (Figure S10). To further clarify the role of metal–support interface, we investigated the catalytic performance of over-coated catalysts prepared by coating Ni-out-ANTs with different Al₂O₃ cycles by ALD (Figure 5A). X-ray photoelectron spectrum results clearly demonstrate the gradual coverage of Ni nanoparticles by ALD Al₂O₃ over-coats (Table S8). For the first few cycles of ALD, Al₂O₃ would deposit preferentially onto specific sites, rather than uniformly blanketing the particles entirely.^[13] The inverse catalysts possess larger metal–support interface. At

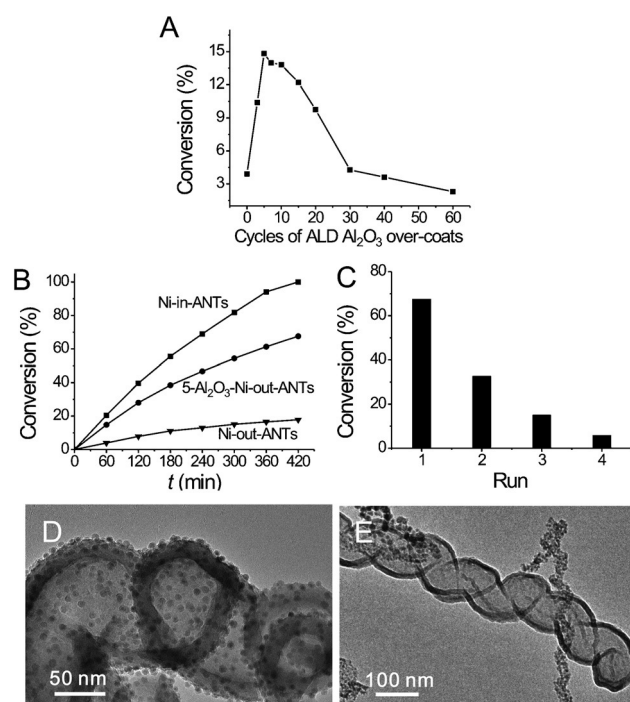


Figure 5. Catalytic performance of the over-coated Ni-out-ANTs catalysts. A) CA conversion obtained after 1 h of CA hydrogenation reaction for over-coated catalysts; B) the evolution of CA conversion with the reaction time; C) the recycling results for 5-Al₂O₃-Ni-out-ANTs; and TEM images of 5-Al₂O₃-Ni-out-ANTs (D) before and (E) after four runs.

the same time, the access of reagents to the embedded Ni nanoparticles is also maintained. Therefore, the inverse catalysts with Al₂O₃ over-coatings in the range of 3–10 cycles show higher activities than the uncoated Ni-out-ANTs. The sample coated with 5 cycles of ALD Al₂O₃ (5-Al₂O₃-Ni-out-ANTs) exhibits the highest activity (Figure 5B). There is no visible morphological change for the coated nanoparticles resulted from the ultrathin coating (Figure 5D). With further increasing cycle numbers of ALD Al₂O₃ (over 30), the particles would be completely encapsulated by Al₂O₃, resulting in decreased catalytic activity, even if such system has larger metal–support interface. This further confirms that the increased Ni–Al₂O₃ interfacial sites are responsible for the greatly enhanced catalytic activity.

Second, from the TEM analysis of the used catalysts (Figure 3C–F), and the Ni contents in the reactant solvent after the reaction, it can be known that the tubular channel structure of the confined catalysts can inhibit the leaching and detachment of Ni nanoparticles of Ni-in-ANTs, consistent with previous results reported in the literature.^[14] As leaching and detachment of Ni nanoparticles will dramatically reduce active surface areas, Ni-in-ANTs with protecting Al₂O₃ shells exhibit dramatically improved catalytic stability than Ni-out-ANTs. To further demonstrate the protective role of the Al₂O₃ shells, 5-Al₂O₃-Ni-out-ANTs sample was reused to test its stability (Figure 5C). The conversion of 5-Al₂O₃-Ni-out-ANTs decreases sharply. Similar to Ni-out-ANTs, vast majority of Ni nanoparticles of 5-Al₂O₃-Ni-out-ANTs are also detached (Figure 5E). The Ni contents in the reactant

solvent after the reaction, measured by ICP-AES, are 1.29 ppm for 5-Al₂O₃-Ni-out-ANTs. Without the sufficiently thick, protective Al₂O₃ shells, the ultrathin-coated catalysts still undergo severe leaching and detachment.

In conclusion, we have demonstrated a facile approach to fabricate a multiply confined Ni-based catalyst with excellent catalytic performance in cinnamaldehyde and nitrobenzene hydrogenation reactions. The Ni nanoparticles are not only confined in Al₂O₃ nanotubes, but also embedded in the cavities of Al₂O₃ interior wall. Our ALD-assisted template method is general,^[15] and can easily be extended for other multiply confined nanoreactors, which may have potential applications in many heterogeneous reactions.

Keywords: atomic layer deposition · hydrogen spillover · hydrogenation reaction · interface · multiply confined catalyst

How to cite: *Angew. Chem. Int. Ed.* **2015**, *54*, 9006–9010
Angew. Chem. **2015**, *127*, 9134–9138

- [1] M. Cargnello, J. J. D. Jaen, J. C. H. Garrido, K. Bakhmutsky, T. Montini, J. J. C. Gamez, R. J. Gorte, P. Fornasiero, *Science* **2012**, *337*, 713–717.
- [2] X. L. Pan, Z. L. Fan, W. Chen, Y. J. Ding, H. Y. Luo, X. H. Bao, *Nat. Mater.* **2007**, *6*, 507–511; X. L. Pan, X. H. Bao, *Acc. Chem. Res.* **2011**, *44*, 553–562.
- [3] X. Yang, X. Yu, L. Z. Long, T. J. Wang, L. L. Ma, L. P. Wu, Y. Bai, X. J. Li, S. J. Liao, *Chem. Commun.* **2014**, *50*, 2794–2796; H. R. Yue, Y. J. Zhao, S. Zhao, B. Wang, X. B. Ma, J. L. Gong, *Nat. Commun.* **2013**, *4*, 7; X. B. Chen, H. Q. Wang, Z. B. Wu, Y. Liu, X. L. Weng, *J. Phys. Chem. C* **2011**, *115*, 17479–17484.
- [4] M. Cargnello, V. V. T. Doan-Nguyen, T. R. Gordon, R. E. Diaz, E. A. Stach, R. J. Gorte, P. Fornasiero, C. B. Murray, *Science* **2013**, *341*, 771–773; I. X. Green, W. J. Tang, M. Neurock, J. T. Yates, *Science* **2011**, *333*, 736–739; Q. Fu, W. X. Li, Y. X. Yao, H. Y. Liu, H. Y. Su, D. Ma, X. K. Gu, L. M. Chen, Z. Wang, H. Zhang, B. Wang, X. H. Bao, *Science* **2010**, *328*, 1141–1144; Y. Yamada, C. K. Tsung, W. Huang, Z. Y. Huo, S. E. Habas, T. Soejima, C. E. Aliaga, G. A. Somorjai, P. D. Yang, *Nat. Chem.* **2011**, *3*, 372–376.
- [5] J. L. Lu, B. S. Fu, M. C. Kung, G. M. Xiao, J. W. Elam, H. H. Kung, P. C. Stair, *Science* **2012**, *335*, 1205–1208; S. M. George, *Chem. Rev.* **2010**, *110*, 111–131; C. P. Canlas, J. L. Lu, N. A. Ray, N. A. Grosso-Giordano, S. Lee, J. W. Elam, R. E. Winans, R. P. Van Duyne, P. C. Stair, J. M. Notestein, *Nat. Chem.* **2012**, *4*, 1030–1036.
- [6] B. J. O'Neill, D. H. K. Jackson, J. Lee, C. Canlas, P. C. Stair, C. L. Marshall, J. W. Elam, T. F. Kuech, J. A. Dumesic, G. W. Huber, *ACS Catal.* **2015**, *5*, 1804–1825; J. Lee, D. H. K. Jackson, T. Li, R. E. Winans, J. A. Dumesic, T. F. Kuech, G. W. Huber, *Energy Environ. Sci.* **2014**, *7*, 1657–1660; R. Lobo, C. L. Marshall, P. J. Dietrich, F. H. Ribeiro, C. Akatay, E. A. Stach, A. Mane, Y. Lei, J. Elam, J. T. Miller, *ACS Catal.* **2012**, *2*, 2316–2326; T. D. Gould, A. M. Lubers, B. T. Neltner, J. V. Carrier, A. W. Weimer, J. L. Falconer, J. W. Medlin, *J. Catal.* **2013**, *303*, 9–15; T. D. Gould, M. M. Montemore, A. M. Lubers, L. D. Ellis, A. W. Weimer, J. L. Falconer, J. W. Medlin, *Appl. Catal. A* **2015**, *492*, 107–116.
- [7] Y. Qin, Y. Kim, L. Zhang, S.-M. Lee, R. B. Yang, A. Pan, K. Mathwig, M. Alexe, U. Gösele, M. Knez, *Small* **2010**, *6*, 910–914; Y. Qin, R. Vogelgesang, M. Eßlinger, W. Sigle, P. van Aken, O. Moutanabbir, M. Knez, *Adv. Funct. Mater.* **2012**, *22*, 5157–5165; C. Marichy, N. Pinna, *Coord. Chem. Rev.* **2013**, *257*, 3232–3253.
- [8] E. J. Shin, A. Spiller, G. Tavoularis, M. A. Keane, *Phys. Chem. Chem. Phys.* **1999**, *1*, 3173–3181.
- [9] R. Kramer, M. Andre, *J. Catal.* **1979**, *58*, 287–295; S. Smeds, T. Salmi, L. P. Lindfors, O. Krause, *Appl. Catal. A* **1996**, *144*, 177–194.
- [10] M. Meng, P. Y. Lin, M. Meng, *Spectrosc. Lett.* **2001**, *34*, 83–92.
- [11] L. R. Baker, G. Kennedy, M. Van Spronsen, A. Hervier, X. J. Cai, S. Y. Chen, L. W. Wang, G. A. Somorjai, *J. Am. Chem. Soc.* **2012**, *134*, 14208–14216; F. B. Su, F. Y. Lee, L. Lv, J. J. Liu, X. N. Tian, X. S. Zhao, *Adv. Funct. Mater.* **2007**, *17*, 1926–1931; M. A. Keane, G. Tavoularis, *React. Kinet. Catal. Lett.* **2003**, *78*, 11–18.
- [12] R. Prins, *Chem. Rev.* **2012**, *112*, 2714–2738.
- [13] J. Lu, B. Liu, N. P. Guisinger, P. C. Stair, J. P. Greeley, J. W. Elam, *Chem. Mater.* **2014**, *26*, 6752–6761; H. Zhang, X.-K. Gu, C. Canlas, A. J. Kropf, P. Aich, J. P. Greeley, J. W. Elam, R. J. Meyers, J. A. Dumesic, P. C. Stair, C. L. Marshall, *Angew. Chem. Int. Ed.* **2014**, *53*, 12132–12136; *Angew. Chem.* **2014**, *126*, 12328–12332.
- [14] G. Park, S. Lee, S. J. Son, S. Shin, *Green Chem.* **2013**, *15*, 3468–3473; J. Ge, Q. Zhang, T. Zhang, Y. Yin, *Angew. Chem. Int. Ed.* **2008**, *47*, 8924–8928; *Angew. Chem.* **2008**, *120*, 9056–9060.
- [15] M. Knez, K. Nielsch, L. Niinistö, *Adv. Mater.* **2007**, *19*, 3425–3438; C. Marichy, M. Bechelany, N. Pinna, *Adv. Mater.* **2012**, *24*, 1017–1032.

Received: April 24, 2015

Revised: May 25, 2015

Published online: July 6, 2015